JACS
JOURNAL OF THE AMERICAN CHEMICAL SOCIETY
Article
pubs.acs.org/JACS

Salt-Excluding Artificial Water Channels Exhibiting Enhanced Dipolar Water and Proton Translocation

Erol Licsandru,[†,∥] Istvan Kocsis,[†,∥] Yue-xiao Shen,[‡,∥] Samuel Murail,[§] Yves-Marie Legrand,[†] Arie van der Lee,[†] Daniel Tsai,[‡] Marc Baaden,[§] Manish Kumar,[‡] and Mihail Barboiu*[,†]

[†]Adaptive Supramolecular Nanosystems Group, Institut Europeen des Membranes, ENSCM-UMII-UMR CNRS 5635, Place Eugene Bataillon CC047, Montpellier, F-34095, France

[‡]Department of Chemical Engineering, Pennsylvania State University, University Park, Pennsylvania 16802, United States

[§]Laboratoire de Biochimie Théorique, CNRS UPR 9080, Institut de Biologie Physico-Chimique, 13 Rue Pierre et Marie Curie, F-75005 Paris, France

Supporting Information

ABSTRACT: Aquaporins (AQPs) are biological water channels known for fast water transport (~10^8–10^9 molecules/s/channel) with ion exclusion. Few synthetic channels have been designed to mimic this high water permeability, and none reject ions at a significant level. Selective water translocation has previously been shown to depend on water-wires spanning the AQP pore that reverse their orientation, combined with correlated channel motions. No quantitative correlation between the dipolar orientation of the water-wires and their effects on water and proton translocation has been reported. Here, we use complementary X-ray structural data, bilayer transport experiments, and molecular dynamics (MD) simulations to gain key insights and quantify transport. We report artificial imidazole-quartet water channels with 2.6 Å pores, similar to AQP channels, that encapsulate oriented dipolar water-wires in a confined chiral conduit. These channels are able to transport ~10^6 water molecules/s, which is within 2 orders of magnitude of AQPs' rates, and reject all ions except protons. The proton conductance is high (~5 H^+/s/channel) and approximately half that of the M2 proton channel at neutral pH. Chirality is a key feature influencing channel efficiency.

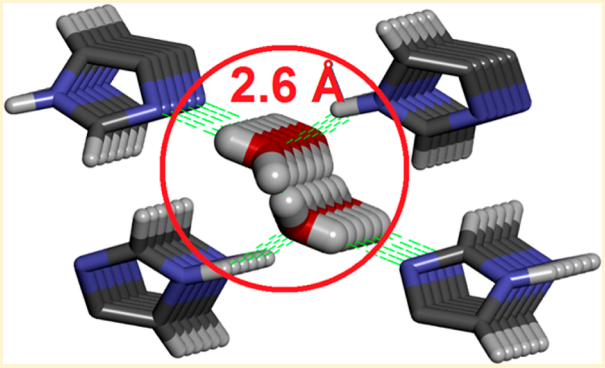

INTRODUCTION

Water is essential for life.[1−3] Under physiological conditions, its molecular-scale hydrodynamics are of crucial relevance to biological functions.[2,3] Changes in water's properties between conventional bulk water and biologically confined water are not limited to size because the water's behavior also becomes quite different.[2] The strong ordering of water molecules at the interface of phospholipid bilayers renders its oriented dipolar structure different from that of bulk water.[4] Moreover, oriented pore-confined water dipoles and correlation motions strongly determine the water and ionic transport rates and the selectivity of biological pores, such as aquaporins (AQPs)[5−7] and gramicidin A.[8]

In this context, we previously reported that natural AQPs can be mimicked using simpler artificial water channels.[9,10] We noted that artificial water channels formed from the supramolecular organization of alkylureido-ethylimidazole compounds (Figure 1) present significant water/proton permeabilities.[11] These compounds form imidazole-quartet (I-quartet) water channels, i.e., stacks of four imidazoles and two water molecules, that can mutually stabilize oriented dipolar water-wires within 2.6 Å pores (Figure 1b). This channel diameter is very close to the narrowest constriction (2.8 Å) observed in very efficient AQP biological water-transport channels.[5]

Here, we show that these novel I-quartet channels exhibit enhanced water and proton transport rates with complete ion rejection. This feature has not been observed for other artificial water channels, which typically have larger pore diameters (4−5 Å) that approach AQPs' permeability but do not achieve any salt rejection.[12−15] We focused on two hypothesized requirements for the realization of more effective artificial water channels using the self-assembling I-quartet motif: (i) More stable synergistically interacting I-quartets and water-wires within the bilayer membrane environment will lead to stabilized channels with higher permeability. (ii) Enhancing the dipolar organization of the water-wires will play an important role in improving water transport and proton translocation.

Received: February 23, 2016
Published: April 10, 2016

DOI: 10.1021/jacs.6b01811
J. Am. Chem. Soc. 2016, 138, 5403−5409

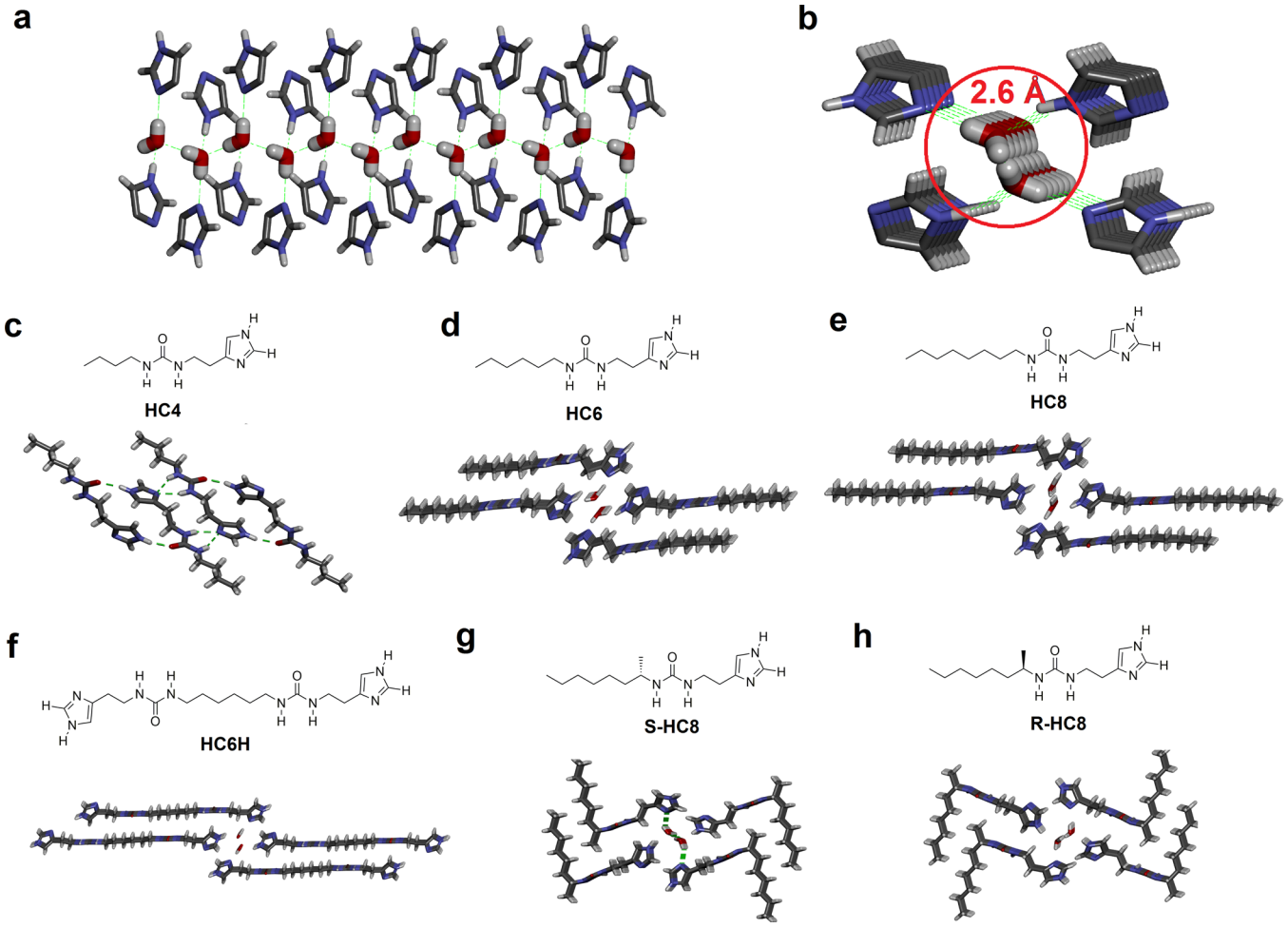

Figure 1. Artificial I-quartet water channels and their chiral isomers pack differently. (a) Side and (b) top views of I-quartet water/proton channels that self-assemble into tetrameric tubular architectures confining dipolar oriented water-wires. Top views of water confining I-quartet channels in stick representations (N, blue; C, gray; O, red; H, white), taken from crystal structures of (c) butylureido-ethylimidazole **HC4**, (d) hexylureido-ethylimidazole **HC6**, (e) octylureido-ethylimidazole **HC8**, (f) bis(ethylimidazole ureido)hexyl **HC6H** (ref 11), (g) *S*-octylureido-ethylimidazole **S-HC8**, and (h) *R*-octylureido-ethylimidazole **R-HC8**. These structures show that packing and self-assembly are dramatically different between chiral and achiral isomers, but all channels have pores with a diameter of 2.6 Å.

RESULTS AND DISCUSSION

Considering the requirements mentioned above, a close examination of the I-quartet structures led us to propose the following novel strategies to control I-quartet water channel formation and stabilization within bilayers: (a) **HC4**, **HC6**, and **HC8** compounds, which have variable alkyl chain lengths, may induce variable morphological hydrophobic stabilization by promoting external wrapping around I-quartets. (b) Chiral **S-HC8** and **R-HC8** compounds may enhance the net chiral self-assembly of I-quartets and thereby strengthen the water dipolar orientation within the channels. Six compounds were prepared for the studies described here (Figure 1c–h).

We treated the corresponding isocyanates with histamine (CH_3CN/*N*,*N*-dimethylacetamide, 120 °C, 5 h) to crystallize **HC4**, **HC6**, **HC8**, **R-HC8**, and **S-HC8** as white powders. The nuclear magnetic resonance (NMR) and electrospray ionization mass spectrometry (ESI-MS) spectra agree with the proposed formulas (Supporting Information). We obtained colorless single crystals of **HC4**, **HC6**, **HC8**, **R-HC8**, and **S-HC8** after recrystallization from water at room temperature. The X-ray structures reveal the expected I-quartets, all (except **HC4**) containing oriented water-wires (Figure 1c–h) (a detailed discussion of the X-ray structural results will be published elsewhere). In all structures, the H atoms of the water molecules present 100% occupancy, and the water molecules of one channel adopt the same dipolar orientation. The overall structures of achiral compounds **HC6** and **HC8** are centrosymmetric, and thus, water-wires of opposite water dipolar orientations are present in successive channels. In contrast to achiral compounds, the noncentrosymmetric structures of chiral compounds **R-HC8** and **S-HC8** show unique dipolar orientations for both channels (Figure S1).

Water-Transport Properties. **HC4**, **HC6**, **HC8**, **R-HC8**, and **S-HC8** assemble into functional water-permeable channels in liposomes. Their water transport rates are strongly dependent on the hydrophobic behaviors of the alkyl tails grafted onto the I-quartets.

We conducted two assays, adding the compounds into the liposomes either before or after lipid mixing. In the first, premix assay, the imidazole I-quartets were mixed with lipids before the liposomes formed. We carefully optimized the lipid systems' phosphatidylcholine, phosphatidylserine, and cholesterol (PC/PS/Chl) composition (molar ratio of 4/1/5) and used a low temperature (10 °C) to maintain low lipid background permeability (~4 μm/s). This low background permeability

DOI: 10.1021/jacs.6b01811
J. Am. Chem. Soc. 2016, 138, 5403–5409

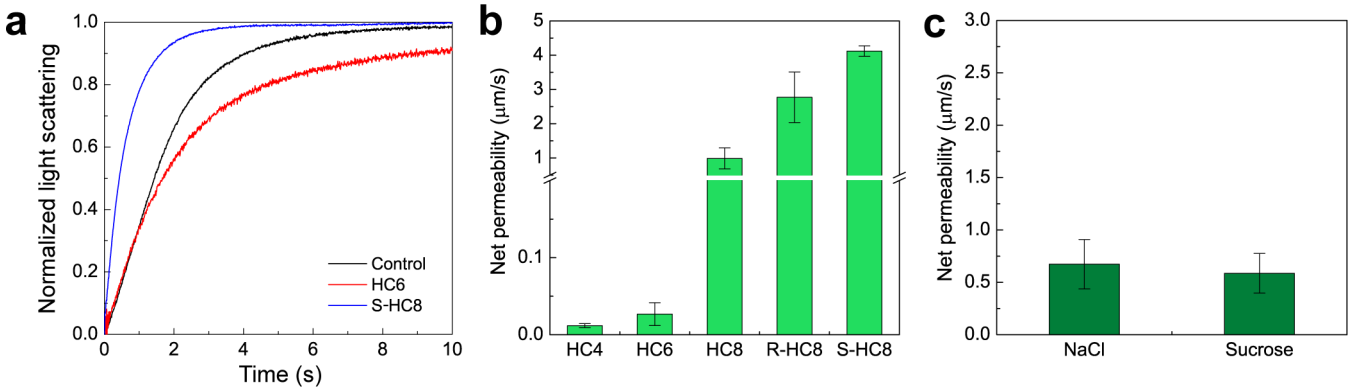

Figure 2. Water-transport activity of I-quartet channels in liposomes. (a) Representative stopped-flow light-scattering experimental traces of liposome premix assays at a CLR (**HC6** and **S-HC8**) of 1 after abrupt exposure to a hypertonic solution of 200 mM NaCl. (b) The water permeabilities of the liposomes containing different I-quartet channels at CLR = 1 were measured under hypertonic conditions from the premix assays. (c) The net water permeability of the **HC8** channels in liposomes at a CLR of 1. The liposomes (1 mg/mL, with a molar ratio of PC/PS/Chl = 4/1/5) were abruptly exposed to a hypertonic solution of 200 mM NaCl or 400 mM sucrose from the premix assays. The data shown in panels b and c are the averages of at least triplicates, and the error bars represent the standard deviation.

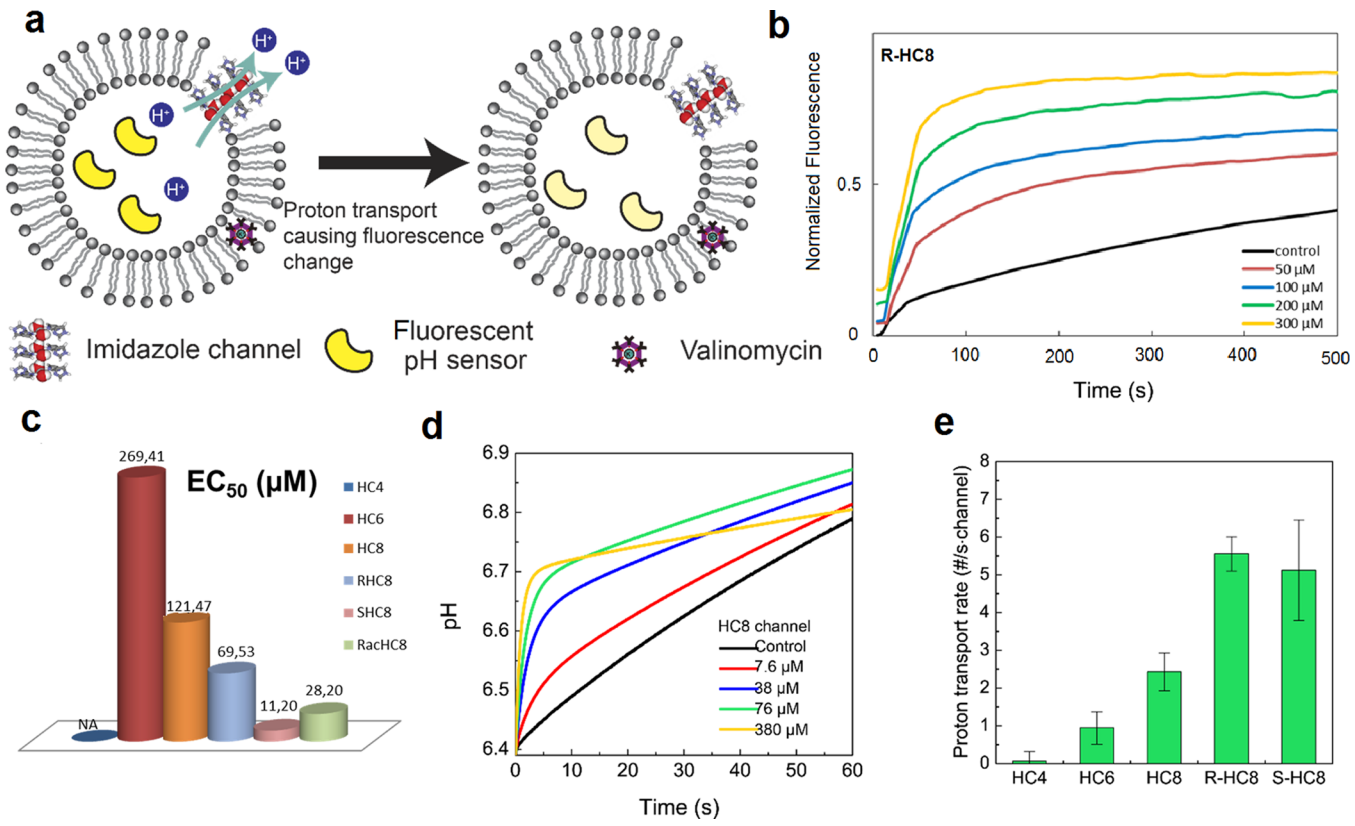

Figure 3. Proton-transport activity of I-quartet channels in liposomes. (a) Liposomes encapsulating pH-sensitive dyes [8-hydroxypyrene-1,3,6-trisulfonic acid (HPTS) and fluorescent dextran] showed fluorescence quenching because of proton export via imidazole channel and K^+ import via valinomicin channel (see Supporting Information for details). (b) Ratiometric fluorescence (I/I_0) curves of the assembled **R-HC8** channels with different channel concentrations in the HPTS assay. The signal was normalized at t = 500 s. (c) Calculated values of EC_{50} (in μM) determined in the HPTS assay, representing the concentration at which the given compound (including racemic **RacHC8**) achieved half of its total transport capabilities. (d) The pH inside the liposomes (pH = 6.4) with the incorporated **HC8** channels increased over time upon exposure to a higher pH environment (pH = 7.4) in kinetic experiments. The experiments were performed on a stopped-flow instrument using a fluorescent D-3305 dextran dye as a pH sensor. Higher **HC8** channel concentrations correlated with faster transport kinetics. (e) Proton-transport rates of different I-quartet channels calculated from the fluorescent dextran assay. The data shown are the averages of at least triplicates, and the error bars represent the standard deviation.

allowed us to resolve the water transport through these channels in stopped-flow light-scattering experiments.[16] Under hypertonic conditions driven by outwardly directed osmotic gradients, the shrinkage of the liposomes increased the light-scattering signal. We fitted a sum of two exponential functions to the latter data.

The kinetics of vesicle shrinkage indicated that some channels had low permeability. Therefore, we implemented a

DOI: 10.1021/jacs.6b01811
J. Am. Chem. Soc. 2016, 138, 5403−5409

method used in recent studies of low-water-permeable systems,[15] including aquaporin AQP0.[17] This analysis yielded two shrinkage rate constants (a larger constant, k_1, and a smaller constant, k_2) and, thus, two permeability values. For **HC4** and **HC6**, k_1 was independent of the compound concentrations, while k_2 increased with the addition of the self-assembled compounds (Figure 2a); this phenomenon was reversed when we added **S-HC8** channels to the vesicles. This result indicates that the superstructures assembled by **HC4** and **HC6** are probably not stable contributing less to the overall bilayer permeability than the lipid background (Figure S2), whereas **HC8** and its chiral isomers **R-HC8** and **S-HC8** increased the overall permeability relative to the background lipid permeability. Therefore, we used the smaller k_2 to calculate the permeabilities for **HC4** and **HC6** assemblies. The larger k_1 was used to characterize the permeabilities of **HC8** and its chiral isomers **R-HC8** and **S-HC8**. The net permeabilities of **HC4** and **HC6** assemblies at a channel-to-lipid weight ratio of 1 (CLR = 1) were 0.012 ± 0.003 and 0.027 ± 0.015 μm/s, respectively, whereas for **HC8** and its chiral isomers **R-HC8** and **S-HC8**, the permeabilities were 1.0 ± 0.3, 2.8 ± 0.7 and 4.1 ± 0.2 μm/s, respectively (Figure 2b). The permeabilities of the I-quartet channels were confirmed in the postmix assay, in which channels were injected into preformed liposomes with the aid of dimethyl sulfoxide (DMSO). The temperature in the postmix experiments was ~20 °C, leading to a relatively high background permeability (~25 μm/s). However, it was still possible to differentiate the channels' contributions to water transport (Figure S3A). We obtained postmix results (Figure S3B) similar to the premix results (Figure 2b). **HC4** and **HC6** assemblies maintained low permeability, but **HC8** and its isomers channels were more permeable toward water.

When dissolved in nonionic surfactants, these I-quartet channels show a unique UV-absorbance signal at 230 nm that we used to calculate the bilayer insertion efficiency (Figure S4). For **HC8** and its chiral isomers **R-HC8** and **S-HC8**, the insertion efficiency was 12.7 ± 2.6%, 68.8 ± 2.9%, and 53.1 ± 6.8%, respectively (Table S1). We calculated the single-channel permeability of each channel type based on the insertion, actual lipid concentration, and channel configuration in the lipids, as previously described[15] (Table S2, see Supporting Information for detailed calculations). In the shrinking mode, **HC8**, **R-HC8**, and **S-HC8** had permeabilities of 1.4(0.4) × 10^6, 7.9(2.1) × 10^5, and 1.5(0.1) × 10^6 water molecules/s/channel, respectively, which are only 2 orders of magnitude lower than that of AQPs (~10^8–10^9 water molecules/s/channel).[4−6]

Proton-Transport Properties. Proton-transport experiments were performed in two independent assays (Figure 3), both of which showed that the transport activity of the I-quartet channels increased with the alkyl chain length.

In the first fluorescence spectroscopy assay,[18] we encapsulated HPTS, a pH-sensitive fluorescent dye, inside vesicles, added channels to the vesicle solution and monitored the fluorescence change over time upon exposure to low pH. The fluorescence intensity was monitored for 500 s, and the fluorescence change rate followed a typical dose−response profile (Figure 3b and Figure S5).

The calculated EC_{50} values showed the effectiveness of each channel−lipid system for proton transport, with lower values indicating higher transport efficiencies.[18] The most active **S-HC8** channels had the lowest EC_{50} (11.2 μM) (Figure 3c and Table S3). On the basis of the EC_{50}, we observed no activity for **HC4**, weak activity for **HC6**, and fairly strong activity for **HC8**, whereas the activities of the **S-HC8** and **R-HC8** optical isomers were 1 order of magnitude higher than those of the achiral **HC8** channels (Table S3 and Figure S5). Tests using an equimolar mixture of the **S-HC8** and **R-HC8** isomers displayed reduced transport activity. All of the determined Hill numbers were below 1, suggesting that the presented channels belong to the type II class (Table S3).[18]

To complement these results, we conducted kinetic measurements of proton-transport activity over 50 s using stopped-flow techniques. We subjected the liposomes with I-quartet channels to a pH gradient across the bilayer and assessed the proton flux by monitoring the fluorescence intensity of encapsulated fluorescent dextran (Figure 3d). As shown in Figure S6, the addition of **HC4** channels did not contribute to the fluorescence response, whereas **HC6** channels slightly increased the proton-exchange rates across the lipid membranes.

In contrast, the kinetics were found to increase by orders of magnitude for **HC8**, and both the **R-HC8** and **S-HC8** channels displayed slightly higher transport kinetics than **HC8**. For **R-HC8**, we observed that the second phase of the fluorescence increase saturated in less than 5 s (Figure S6). This behavior was significantly different from that of **S-HC8**, which showed continuously increasing fluorescence without saturation as the concentration increased (especially for the 380 μM sample). This observation implies that the **R-HC8** chiral channels had an immediately higher kinetic response to the proton transport, whereas the **S-HC8** chiral channels required time to exhibit dynamic behaviors within the lipid bilayer, leading to slower initial transport rates and, subsequently, higher proton permeability, as observed for the proton activity over long periods of time.

We further estimated that the single-channel proton transport rates (Figure 3e, see the Supporting Information for detailed calculations) of the **HC4**, **HC6**, **HC8**, **R-HC8**, and **S-HC8** channels were 0.1 ± 0.2, 0.9 ± 0.4, 2.4 ± 0.5, 5.6 ± 0.5, and 5.1 ± 1.3 protons/s/channel, respectively. The proton fluxes (especially for the **R-HC8** and **S-HC8** channels) were similar to that of the M2 proton channel determined under the same experimental conditions at pH = 7.[19] Our initial assumption, which postulated that water-wires are structural descriptors that could be used to understand the M2 channel's proton-transport function,[11] is confirmed by the proton fluxes observed in these systems. A recent computational study[20] based on a high-resolution structure of the M2 proton channel quantified how water-wires factor into the process of proton translocation.

The bilayer membrane transport experiments allowed us to draw the following conclusions:

(i) Water/proton transport activities increase substantially as the grafted alkyl chain length increases (**HC4** < **HC6** ≪ **HC8**), implying a more stable hydrophobic shell wrapping around the I-quartets at the interface with the bilayers. The increased efficiency of the I-quartets could be synergistically attributed to the enhanced hydrophobic stabilization of the channels within the bilayer membrane environment based on the optimal molecular packing of the hydrophobic tails. Although **HC4** and **HC6** show channel structures in crystals forms, they did not behave like highly water-permeable or proton-conductive channels in bilayer membranes. This is a structure−activity argument and is related to their stability in the bilayer membrane which will be further described in the simulation

DOI: 10.1021/jacs.6b01811
J. Am. Chem. Soc. 2016, 138, 5403−5409

part below. Indeed, the tail length seemed to be optimal for *octyl* chains (longer chains led to precipitation when mixed with lipids). Molecular dynamics (MD) simulations described subsequently support this assertion.

(ii) The I-quartets of the chiral **R-HC8** and **S-HC8** compounds show a unique dipolar orientation of water-wires within all the channels and exhibit high water/proton conductivities, with a preference for the **S-HC8** isomer. The explanation may relate to the channel chirality: The chiral **S-HC8** channels may be more compatible with the naturally occurring chiral L-lipids than the isostructural **HC8** channels.[21] Table S1 shows insertion efficiency measurements supporting this assertion. Moreover, we noted increased water/proton activity of the chiral **R-HC8** I-quartets under kinetic conditions, whereas the overall conductivity of the **S-HC8** I-quartets was higher under thermodynamic equilibrium conditions.

Ion (Na^+ and Cl^-) transport across the bilayer membranes incorporating the **HC8** and **S-HC8** I-quartet channels was assessed using standard fluorescence procedures, and no response versus the control experiment and a lack of variation of the transport activity with the concentration of I-quartets (Figure S7) were observed. In addition, the apparent permeability showed no significant difference between the two hypertonic solutions (+200 mM NaCl). We calculated the reflection coefficient for NaCl as the ratio of the measured water permeability in the presence of salt to that in the presence of a completely retained sucrose osmolyte. The coefficient (113 ± 15%, n = 4) indicated that this channel (**HC8**) achieved approximately 100% salt rejection in the current lipid system.[22]

Molecular Simulations. We performed MD simulations to understand the structure/activity relationships of the artificial water channels formed by **HC6**, **HC8**, **R-HC8**, and **S-HC8** I-quartets. We embedded small (ca. 3 nm wide) I-quartet channel patches based on the X-ray structures in a lipid bilayer environment with the same composition as that used in the experiments to begin each simulation (Table S4). The MD results showed that I-quartets preferentially located within the bilayer membrane region and stabilized water channels in all simulations, although the degrees of water occupancy, transport, and structuring varied. We observed that the structural dynamics of I-quartet channels was dependent on the lateral pressure applied to the membrane, with higher pressure favoring the structuring of the water-wires and stabilizing the structure of the I-quartets (Figure S8). For our comparative investigations, we chose 10 atm of lateral pressure as a good compromise to maintain aggregate structuring and allow us to achieve reasonable sampling and water activity statistics (Figures S9 and S10) within the simulation's microsecond time scale.

We observed that the chiral **R-HC8** and **S-HC8** I-quartets form the most stable and structured systems, followed by the significantly less structured **HC8** I-quartet (Figure 4a), in accordance with the experimentally observed bilayer insertion and water/proton-conduction behaviors. The latter instability echoes the influence of the alkyl chain length, with improved packing and a more stable hydrophobic shell formation occurring with longer chains. After the initial relaxation, the simulations of the chiral **S-HC8** and **R-HC8** I-quartet systems show slightly twisted superstructures. The twist angles between the upper and lower leaflets were 18.4° ± 2.1 and 7.6° ± 4.0, respectively, over the second half of the simulation, whereas the twist was negligible for **HC6** and **HC8** (Figure S11). Both the

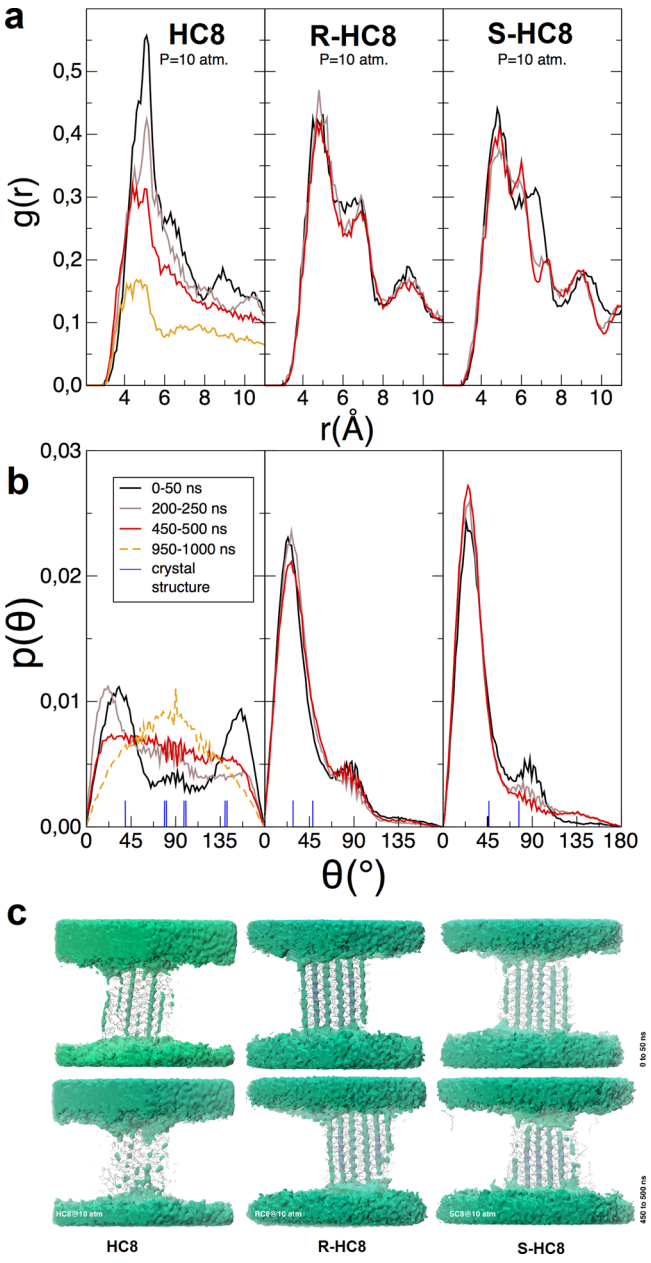

Figure 4. MD simulations of the I-quartet channels illustrate how the hydrophobic chain length and chirality influence the structuring of the hydrophobic shells around the water-wires in these artificial channels. Data for **HC8**, **R-HC8**, and **S-HC8** channels at 10 atm are shown. (a) IMIDN17 atom radial distribution function for various time spans of each simulation. (b) Cumulative water dipole orientation distributions within the membrane region at various time spans indicate the highest stabilization for the **S-HC8** channels. (c) Isosurface water density within the membrane region cumulated at the beginning (0−50 ns) and the end (400−450 ns) of the simulations of the **HC8**, **R-HC8**, and **S-HC8** channels at 10 atm.

chiral **S-HC8** and **R-HC8** I-quartets with bent structures contained more structured water-wires than the achiral linear **HC8** and **HC6** I-quartets and exhibited higher stability over time (Figures 4, S12, and S13). We quantified the water-wire preservation by analyzing the water dipole orientations within the membrane, as shown in Figure 4b. The **R-HC8** and **S-HC8** systems show a strong preference for a dipole orientation of ~25°, whereas the **HC8** system shows two orientations at the

DOI: 10.1021/jacs.6b01811
J. Am. Chem. Soc. 2016, 138, 5403−5409

beginning of the simulation and tends toward a near-random distribution at the end. The dipole orientation is slightly more pronounced for the **S-HC8** system compared to the **R-HC8** system (Figure S14).

The MD simulations provided further insights into the dynamic behaviors of the I-quartets and water molecules under confined conditions in a lipid bilayer environment. Although the **HC6**, **HC8**, **R-HC8**, and **S-HC8** molecules deviate from their initial positions, the chiral channels preserve their overall integrity, but the achiral ones lose it. Water transport is another important property of these aggregates. Because the model system size is small, we focused on the central channels to make inferences regarding water-transport trends.

These buried paths are less affected by boundary effects at the lipid/I-quartet interface than the peripheral ones. Despite the limited time scale and the absence of an osmotic driving force, we observed significant spontaneous permeation through **R-HC8** compared to the reference **HC8** system (Figure S15), whereas the incipient water transport in the **S-HC8** channels was near zero. This observation is consistent with the experimental results, shedding light on the fast kinetic response of the **R-HC8** channels presenting a certain motional behavior within the bilayer. In contrast, the slower thermodynamic response is related to the incipient stability of the **S-HC8** channels within the L-lipids and needs time to reach dynamic behaviors and to achieve functional water permeability within the bilayer. This is highlighting the importance of the dynamics of the channels superstructures which may remain stable and dynamic enough to allow water motion inside the water channels.

CONCLUSIONS

Overall, the self-assembled I-quartet channels, obtained using simple chemistry, can be assembled into robust artificial water channels and remain stable in lipid membranes. The complementary MD and experimental studies presented here provide the first molecular-level insights into the functional dynamics of artificial water channels in the lipid membrane environment. Their permeability ($\sim 10^6$ water molecules/s/channel) is only 2 orders of magnitude lower than that of AQPs. The I-quartets are dimensionally compatible with encapsulated water molecules, both measuring 2.6−2.8 Å in diameter, which is very similar to the narrowest pore dimension of natural AQPs.[4−6] Accordingly, we postulate that a pore with a diameter of ∼3 Å is a critical prerequisite for salt-ion-selective water translocation. The observed total ionic-exclusion behavior of these channels suggests that they hold significant promise for the incipient development of the first innovative materials based on artificial synthetic scaffolds mimicking the functions of natural water channels.

These channels' lipid affinities influence their stability in the membrane and consequently constitute a means to tune their activity. In all cases, the activity of the chiral I-quartets is superior to that of the isostructural nonchiral I-quartets. This observation suggests that the lipids may exert a conformational preference, stabilizing the chiral superstructures. Additionally, the chiral I-quartets preserve the total dipolar orientation and ordering of the water-wires. The mutual interactions between the inner chiral surfaces of the I-quartets, which result in the total dipolar orientation of the water-wires,[23,24] probably impose an internal dielectric polarization within the pore, acting as a constitutive driving force and activating water and proton translocation in a way that differs significantly from their nonoriented or bulk counterparts.

These findings may inspire the incorporation of I-quartets into future membrane materials for desalination and water-purification applications.[25]

ASSOCIATED CONTENT

Supporting Information

The Supporting Information is available free of charge on the ACS Publications website at DOI: 10.1021/jacs.6b01811.

Materials and Methods, Figures S1−S15, Tables S1−S4, and supplementary references (PDF)
X-ray crystal details for **HC4** (CIF)
X-ray crystal details for **HC6** (CIF)
X-ray crystal details for **HC8** (CIF)
X-ray crystal details for **HC6H** (CIF)
X-ray crystal details for **S-HC8** (CIF)
X-ray crystal details for **R-HC8** (CIF)

AUTHOR INFORMATION

Corresponding Author

*mihail-dumitru.barboiu@univ-montp2.fr

Author Contributions

‖E.L., I.K., and Y.-x.S. contributed equally.

Notes

The authors declare no competing financial interest.

ACKNOWLEDGMENTS

This work was supported by funds from ITN DYNANO, PITN-GA-2011-289033 (http://www.dynano.eu).

REFERENCES

(1) Ball, P. *Chem. Rev.* **2008**, *108*, 74−108.
(2) Zhong, D.; Pal, S. K.; Zewail, A. H. *Chem. Phys. Lett.* **2011**, *503*, 1−11.
(3) Pal, S. K.; Zewail, A. H. *Chem. Rev.* **2004**, *104*, 2099−2123.
(4) Cheng, J. X.; Pautot, S.; Weitz, D. A.; Xie, X. S. *Proc. Natl. Acad. Sci. U. S. A.* **2003**, *100*, 9826−9830.
(5) Agre, P. *Angew. Chem., Int. Ed.* **2004**, *43*, 4278−4290.
(6) Kosinska Eriksson, U. K.; Fischer, G.; Friemann, R.; Enkavi, G.; Tajkhorshid, E.; Neutze, R. *Science* **2013**, *340*, 1346−1349.
(7) Sundaresan, V.; Abrol, R. *Chirality* **2005**, *17*, S30−S39.
(8) Allen, T. W.; Andersen, O. S.; Roux, B. *Proc. Natl. Acad. Sci. U. S. A.* **2004**, *101*, 117−122.
(9) Barboiu, M.; Gilles, A. *Acc. Chem. Res.* **2013**, *46*, 2814−2823.
(10) Barboiu, M. *Angew. Chem., Int. Ed.* **2012**, *51*, 11674−11676.
(11) Le Duc, Y.; Michau, M.; Gilles, A.; Gence, V.; Legrand, Y.-M.; van der Lee, A.; Tingry, S.; Barboiu, M. *Angew. Chem., Int. Ed.* **2011**, *50*, 11366−11372.
(12) Zhao, H.; Sheng, S.; Hong, Y.; Zeng, H. *J. Am. Chem. Soc.* **2014**, *136*, 14270−14276.
(13) Barboiu, M.; Le Duc, Y.; Gilles, A.; Cazade, P.-A.; Michau, M.; Legrand, Y.-M.; van der Lee, A.; Coasne, B.; Parvizi, P.; Post, J.; Fyles, T. *Nat. Commun.* **2014**, *5*, 4142.
(14) Hu, X. B.; Chen, Z.; Tang, G.; Hou, J. L.; Li, Z. T. *J. Am. Chem. Soc.* **2012**, *134*, 8384−8387.
(15) Shen, Y. X.; Si, W.; Erbakan, M.; Decker, K.; De Zorzi, R.; Saboe, P. O.; Kang, Y. J.; Majd, S.; Butler, P. J.; Walz, T.; Aksimentiev, A.; Hou, J. L.; Kumar, M. *Proc. Natl. Acad. Sci. U. S. A.* **2015**, *112*, 9810−9815.
(16) Borgnia, M. J.; Kozono, D.; Calamita, G.; Maloney, P. C.; Agre, P. *J. Mol. Biol.* **1999**, *291*, 1169−1179.
(17) Tong, J.; Canty, J. T.; Briggs, M. M.; McIntosh, T. J. *Exp. Eye Res.* **2013**, *113*, 32−40.

DOI: 10.1021/jacs.6b01811
J. Am. Chem. Soc. 2016, 138, 5403−5409

(18) Matile, S.; Sakai, N. In *Analytical Methods in Supramolecular Chemistry*; Schalley, C. A., Ed.; Wiley-VCH: Weinheim, Germany, 2007; pp 381−418.
(19) Leiding, T.; Wang, J.; Martinsson, J.; DeGrado, W. F.; Årsköld, S. P. *Proc. Natl. Acad. Sci. U. S. A.* **2010**, *107*, 15409−15414.
(20) Liang, R.; Li, H.; Swanson, J. M. J.; Voth, G. A. *Proc. Natl. Acad. Sci. U. S. A.* **2014**, *111*, 9396−9401.
(21) Ishigami, T.; Suga, K.; Umakoshi, H. *ACS Appl. Mater. Interfaces* **2015**, *7*, 21065−21072.
(22) Meinild, A.-K.; Klaerke, D. A.; Zeuthen, T. *J. Biol. Chem.* **1998**, *273*, 32446−32451.
(23) Joseph, S.; Aluru, N. R. *Nano Lett.* **2008**, *8*, 452−458.
(24) Dellago, C.; Naor, M. M.; Hummer, G. *Phys. Rev. Lett.* **2003**, *90*, 105902.
(25) Shen, Y-x.; Saboe, P. O.; Sines, I. T.; Erbakan, M.; Kumar, M. *J. Membr. Sci.* **2014**, *454*, 359−381.

DOI: 10.1021/jacs.6b01811
J. Am. Chem. Soc. 2016, 138, 5403−5409